Molecular Catalysis xxx (2017) xxx–xxx

Contents lists available at ScienceDirect

Molecular Catalysis

journal homepage: www.elsevier.com/locate/mcat

Dispersion of nanosized ceria-terbia solid solutions over silica surface: Evaluation of structural characteristics and catalytic activity

Abu Taleb Miah, Pranjal Saikia*

Department of Applied Sciences (Chemical Science Division), Gauhati University, Guwahati,781014, Assam, India

ARTICLE INFO

Article history:
Received 26 August 2017
Received in revised form
11 November 2017
Accepted 13 November 2017
Available online xxx

Keywords:
Ceria-terbia solid solution
Thermal stability
Dehydration
4-methylpentan-2-ol
4-methylpent-1-ene

ABSTRACT

In this work, we investigated the dispersion effects of nanosized ceria-terbia solid solutions over silica surface in terms of structural characteristics and catalytic activity. The dispersion process was carried out *via* a soft chemical route using colloidal silica precursor and nitrate precursors of cerium and terbium. The structural features were elucidated by means of analytical techniques namely TGA, BET surface area, XRD, Raman Spectroscopy, UV–vis DRS, TEM, XPS, and TPR-TPO. The catalyst samples were subjected to thermal treatments at different temperatures ranging from 773 to 1073 K to understand the influence of silica support on dispersion, textural properties, and thermal stability. Catalytic activity was evaluated for selective dehydration of 4-methylpentan-2-ol to 4-methylpent-1-ene in the vapor phase at atmospheric pressure. The silica supported ceria-terbia catalyst exhibited better dehydration activity as well as selectivity in comparison to the unsupported catalyst. The catalytic properties were found to be dependent on structural features of the prepared catalyst samples.

1. Introduction

Since its inception as the oxygen storage component in catalytic converters by Ford Motor Company, nanosized cerium oxide (ceria, CeO_2) has been known to be an unrivaled component in three-way-catalysts (TWCs) and is currently an attractive catalyst or a support for a variety of catalytic applications [1,2]. The unique property making ceria extraordinarily viable is its oxygen storage and release capacity *via* the Ce^{4+}/Ce^{3+} redox shuttle under oxidizing and reducing environments, respectively [1–5]. Primarily, ceria was recognized as a promising material, because it maintains a cubic fluorite crystal structure even during the alternate storage and release of oxygen with small volume change. However, due to severe loss of its textural characteristics and oxygen storage capacity (OSC) at elevated temperatures, its use in controlling the emissions of toxic pollutants from automotive exhaust is restricted [3]. Two strategies are particularly effective for resolving this critical problem. One is modification of ceria by preparing its mixed oxides or solid solutions with transition metals and other rare-earth elements, and another is exploitation of thermally stable inert supports [1–3,4,6]. Captivatingly, both the strategies have come up with improved thermal/textural properties and catalytic activities for ceria nanostructures. For instance, prominent mixed oxides of ceria such as CeO_2-ZrO_2, CeO_2-HfO_2, CeO_2-La_2O_3, CeO_2-TiO_2, CeO_2-TbO_2, CeO_2-PrO_2, etc. have been known in view of both structural characteristics and catalytic activities compared to pure ceria in different applications [3,6–10].

Due to chemical inertness, high specific surface area and high thermal stability, silica is widely exploited as a support for stabilizing different metal nanoparticles and metal oxides [11,12]. It is revealed that the dispersion of nanosized ceria and/or ceria-based mixed oxides over the surface of silica, transition alumina, or titania results in significant improvement of the physical as well as chemical properties without changing the thermal and mechanical properties of the mixed oxide material [11]. Mention worthy that amorphous silica outperforms the ability of alumina and titania towards the stabilization of the ceria-based mixed oxides against sintering during the high temperature operations [13]. Furthermore, compared to the bulk oxides, the silica supported ceria-based mixed oxides possesses more active surface area and stability due to better dispersion of the catalytically active ceria-based phases on the support surface. As a consequence, the oxygen exchange rate experiences an enhancement that leads to a remarkable increase in the reactivity [6,13]. These facts grow intense motivation towards using silica as the support material for other ceria-based materials.

Apart from the well-known redox behavior, acid-base property is another intriguing feature of ceria-based catalysts. Generally, different techniques employed to explore the acid-base properties of ceria suggest strong basicity and weak acidity caused by the highly mobile surface O^{2-} ions and cerium cations, respectively [11,14].

* Corresponding author.
E-mail addresses: psjorhat@gmail.com, pranjalsaikia@gauhati.ac.in (P. Saikia).

http://dx.doi.org/10.1016/j.mcat.2017.11.020
2468-8231/

Introduction of metal dopants into the CeO_2 lattice generates oxygen vacancy defects and increases the acidity or basicity of CeO_2 [4,10,15,16]. Finding an appropriate metal for doping is greatly important and a lot of attention should be focused on this issue. By making the use of acid-base as well as the redox properties, ceria and/or ceria-based materials can catalyze the transformation of diverse organic molecules. For instance, dehydration, dehydrogenation and dimerization of alcohols, condensation of aldehydes, ketonization of acids, hydrogenation of olefins, esterification of alcohols, and transesterification of esters were found to be effectively catalyzed by ceria-based catalysts [11,17–20].

Selective dehydration of 4-methylpentan-2-ol is technologically very important as the exclusive product 4-methylpent-1-ene is used as the starting material for manufacturing thermoplastic polymers [21]. However, the dehydration reaction often leads to the formation of undesired product, 4-methylpent-2-ene with trace amounts of C_6-alkenes [4,22]. Besides, the dehydration reaction may be simultaneously accompanied by dehydrogenation which produces 4-methylpentan-2-one along with higher ketones in negligible amounts [4,22]. Hence, product selectivity remains a fundamental issue particularly in alcohol dehydration and tremendous effort has been directed to achieve satisfactory selectivity. It is believed that the strength of acid- and base-sites govern the competition among products of 4-methylpentan-2-ol dehydration [17]. Pure ceria predominantly produces 2-alkene as the alcohol dehydration product. However, binary ceria-based mixed oxide solid solutions reveal good catalytic activity as well as high selectivity to 1-alkene in the dehydration of secondary alcohols [8,23,24]. It is reported that dispersion of ceria-based nano-oxide catalysts, namely, $Ce_xZr_{1-x}O_2$, $Ce_{0.8}Hf_{0.2}O_2$, and CeO_2-La_2O_3 over silica amazingly increase their catalytic activity in selective dehydration of 4-methylpentan-2-ol [4,24,25]. Reddy and co-workers reported the efficiency of alumina supported ceria-terbia solid solution in comparison to unsupported ceria-terbia toward enhancement of OSC and CO oxidation ability [3]. In view of this, investigation on ceria-terbia solid solutions supported on silica is vital for making a rational comparison to the previously reported work. To the best of our knowledge, very little research endeavor has been dedicated toward investigation of acid-base characteristics of ceria-based nanostructures correlating their catalytic activity, and particularly, no report could be found on SiO_2 supported CeO_2-TbO_2 composite oxides so far.

Against the abovementioned background, we have undertaken the present investigation to understand the dispersion effects of CeO_2-TbO_2 composite oxide over the surface of silica obtained from colloidal dispersion because of its certain advantages. First, the colloidal dispersion is much less reactive towards the catalytic material, and therefore, solid-state reactions are slightly less likely to occur with the colloidal materials than with the co-precipitated materials from soluble salts. Second, the particles of the colloid are larger than the particles of the co-precipitated salt. This has the feature of making larger pores and a more open structure for the final catalyst. In this work, we therefore aim to evaluate the physicochemical characteristics, nanostructural evolution, and catalytic activity of CeO_2-TbO_2/SiO_2 ternary oxide catalyst where ceria-terbia mixed oxide acts as a promoter and silica forms part of the substrate.

2. Experimental

2.1. Preparation of catalysts

The silica supported ceria-terbia (*i.e.*, CeO_2-TbO_2/SiO_2) catalyst (CTS; CeO_2:TbO_2:SiO_2 = 80:20:100 mol% based on oxides) was synthesized by a deposition co-precipitation method. Nitrate precursors, ammonium cerium(IV) nitrate (Himedia) and terbium(IV) nitrate (Himedia) in requisite quantities were dissolved separately in double distilled water under mild stirring conditions and mixed together. Upon complete mixing, required quantity of colloidal silica (Ludox 40 wt.%, Aldrich, AR grade) was added to the abovementioned mixture solution under vigorous stirring. Dilute aqueous ammonia solution was subsequently added dropwise until the precipitation was complete (pH = ~8.5). The resulting precipitate was carefully filtered off and washed with distilled water until it became free from anion impurities. The accumulated paste was left for overnight drying in a hood. Subsequently, the solid product was dried in an oven at 393 K for 12 h, and crushed it using an agate mortar to obtain fine powders. Finally, the dried sample was calcined at 773 K for 5 h in air atmosphere. Some portions of this sample were again heated at 873, 973, and 1073 K, respectively for 5 h in air atmosphere for investigating the thermal stability of the samples. A heating rate of 5 K/min was maintained during all the calcination processes. For comparison, unsupported CeO_2-TbO_2 (CT; 80:20 mol% based on oxides) was also prepared by same method, annealed at different temperatures, characterized and evaluated for catalytic usefulness.

2.2. Characterization of catalysts

The thermogravimetric measurements were carried out on a Mettler-Toledo TG-SDTA instrument. The catalyst sample was heated from ambient to 1273 K under nitrogen flow at the heating rate of 10 °C per minute. The BET surface areas were determined by N_2 physisorption at liquid N_2 temperature on a Micromeritics Gemini 2360 instrument using a thermal conductivity detector (TCD). Prior to analysis, the samples were oven dried at 393 K for 12 h to remove the surface adsorbed moisture contents and finally flushed with argon gas for 2 h. The powder X-ray diffraction (XRD) patterns were recorded on a Rigaku Multiflex instrument using nickel-filtered CuKα (0.15418 nm) radiation source and a scintillation counter detector. The intensity data were collected over a 2θ range of 10–80° with a step size of 0.02° and a collection time of 2 s per step. Average particle sizes were calculated using Scherrer equation and the cell parameter 'a' of various catalysts was determined by a standard cubic indexation method using the most intense (111) peak. The Raman spectra were recorded on a DILOR XY spectrometer equipped with a confocal microscope and liquid N_2 cooled charge-coupled device (CCD) detector. Samples were excited with the emission line at 325 nm from He-Cd laser (Melles Griot Laser) under the microscope with the diameter of the analyzed spot being ~1 μm. The wavenumber values obtained from the spectra are precise to within 2 cm^{-1}. UV–vis diffuse reflectance spectra were collected on a UV–vis spectrophotometer, Model U-4100 spectrophotometer (solid). $BaSO_4$ was used as the reference material and the spectra were recorded in the wavelength range from 200 to 800 nm. XPS investigations were carried out on a Shimadzu (ESCA 3400) Spectrometer by using MgKα (1253.6 eV) radiation as the excitation source. The samples were dried and evacuated at high vacuum before analysis and then introduced into the analysis chamber. The recorded XPS spectra were charge corrected with respect to the binding energy of C 1s peak at 284.6 eV. Quantitative analysis of atomic ratios was accomplished by determining the elemental peak areas as reported in our previous literature [3]. Transmission electron microscopic (TEM) investigations were made on a JEM-2100 (JEOL) instrument equipped with a slow scan CCD camera and at an accelerating voltage of 200 kV. Samples were prepared by ultrasonic dispersion in ethanol and deposited onto carbon-coated copper grids. The TPR-TPO measurements were performed using a micro-reactor coupled to a TCD. Oxygen storage capacity (OSC) was measured from the oxygen release characteristics of the sample in the temperature

Please cite this article in press as: A.T. Miah, P. Saikia, Dispersion of nanosized ceria-terbia solid solutions over silica surface: Evaluation of structural characteristics and catalytic activity, Mol. Catal. (2017), http://dx.doi.org/10.1016/j.mcat.2017.11.020

region 573–1073 K *via* a thermogravimetric method. The detailed procedures for TPR-TPO and OSC measurements have been provided in the electronic supplementary information (ESI) section.

2.3. Evaluation of catalytic activity

Catalytic activities of the prepared samples were evaluated for dehydration of 4-methylpentan-2-ol. The experiments were carried out in the temperature region of 523–673 K, in a down flow fixed-bed microreactor heated by means of a tubular furnace as described earlier [22,25]. In a typical experiment, 0.5 g of catalyst diluted with quartz fractions was placed vertically inside a tubular furnace. Prior to the reaction, the catalyst was heat treated at 773 K for 5 h using CO_2-free airflow. The 4-methylpentan-2-ol was fed into the vaporizer at a flow rate of 1.5 ml h^{-1} through a N_2 stream flows at the rate of 60–70 ml min^{-1}. The condensed liquid products were collected in ice-cold freezing traps and then analyzed by a gas chromatograph equipped with BP-20 (wax) capillary column and a flame ionization detector (FID) to monitor the evolution of the reaction. The conversion and product selectivity were calculated as per the procedure described elsewhere [22,24].

3. Results and discussion

3.1. Characterization of catalysts

To gain information on the role of silica support against sintering and decomposition behavior of ceria-terbia solid solution thermogravimetric analysis (TGA) was performed. The thermograms between 273 and 1273 K, pertaining to TG analysis (ESI, Fig. E1) of the uncalcined CTS composite oxide revealed one major and two minor weight loss peaks. The major weight loss peak is broad in nature and appears at low temperature region, which can be assigned to the loss of non-dissociative adsorbed water. The minor weight losses encompass the intermediate as well as high temperature regions. The weight loss in the intermediate region is caused by the loss of water present in the micropores of the gel. On the other hand, the other minor weight loss peak noted at the highest temperature region is due to dehydroxylation of the surface. This observation indicates that the weight loss of CTS sample from ambient condition to ~830 K was about 15%, whereas from 830 to 1273 K it was about 0.5–1% only. Based on TGA informations, it can be demonstrated that the silica supported ceria-terbia composite oxide is thermally quite stable and could be used in high temperature applications.

The N_2 BET surface areas of various samples calcined at different temperatures are presented in Table 1. The CTS sample calcined at 773 K exhibited a very high surface area of 170 m^2 g^{-1}. Evidently, the specific surface area of the CTS sample experienced a gradual fall with increase in calcination temperature from 773 to 1073 K. However, preservation of a fairly high surface area of 110 m^2 g^{-1} even after calcination at 1073 K is an amazing observation. It is known that the surface area of the supported ceria-terbia samples and their resistance against thermal sintering robustly rely on the synthetic approaches [3]. The procedure that we followed in the present investigation was found to be highly effective in stabilizing the surface area of the supported ceria-terbia composite oxides.

Powder XRD patterns of the CTS samples calcined in the temperature range from 773 to 1073 K along with pure ceria and terbia (calcined at 773 K) have been presented in Fig. 1. The patterns reveal the formation of a cubic fluorite type phase with the composition $Ce_{0.8}Tb_{0.2}O_2$ for all CTS samples. As can be seen, though the intensity of the diffraction lines increases with increasing calcination temperature, the peak positions remain unaltered. At lower calcination temperatures the crystallite size (measured by Scherrer equation) is normally small and the surface area is large (Table 1). As per earlier literature report, the evolution of different phases leading to phase segregation may occur at higher calcination temperatures [26]. This is attributed to smaller surface energy contribution results from the minimization of surface area at high temperature [26,27]. Intriguingly, no phase segregation could be observed in the present diffraction patterns despite after calcination at 1073 K.

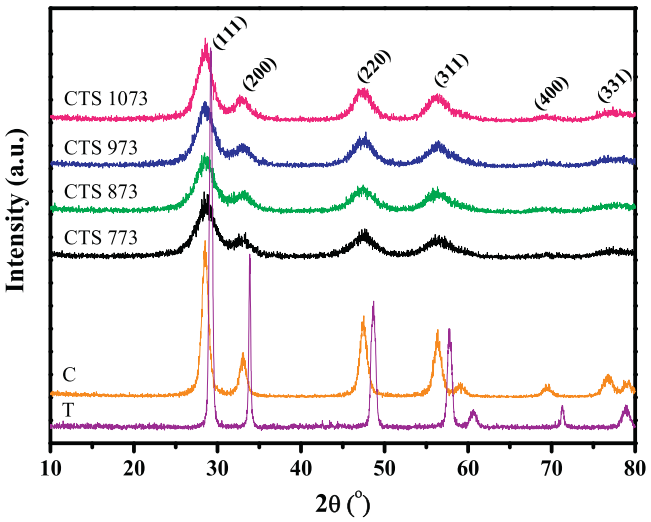

Fig. 1. Powder XRD patterns of $CeO_2 - TbO_2/SiO_2$ (CTS) samples calcined at different temperatures along with 773 K calcined ceria (C) and terbia (T).

The patterns also disclosed a fascinating information that there is no further compound formation such as $Ce_{9.33}(SiO_4)_6O_2$, and $CeSiO_4$ between various component oxides (CeO_2, TbO_2, and SiO_2) of the sample as reported in the literature [28,29]. This could be attributed to various factors like, utilization of inert colloidal silica as the support, strong interaction between the oxides of Ce and Tb to form solid solutions, and exploitation of lower calcination temperatures [26]. Within the detection limits of the XRD technique, there was no evidence about the presence of terbia phases. In addition, any XRD features relating to silica were also not identified, representing amorphous nature of the support.

Using the most intense CeO_2 (111) diffraction peak, calculation of cell parameters 'a' for the synthesized samples was carried out [30,31]. The corresponding 'a' values for the samples calcined at different temperatures are summarized in Table 1. As can be observed, the conformity of the cell 'a' parameter values with increasing calcination temperature signifies the stable nature of the compound. However, integration of terbium ions into the ceria lattice results in the shrinking of the unit cell size in accordance with Vegard's law [3]. This observation clearly reveals direct dependency of the lattice parameter of a solid solution to the atomic percent of the solute present [32–34]. The substitution of Ce^{4+} ions by Tb^{4+} and Tb^{3+} ions leads to a respective reduction and enhancement of the crystalline lattice parameter, which is attributed to the relatively smaller and larger ionic radius of Tb^{4+} (0.88 Å) and Tb^{3+} (1.04 Å) than Ce^{4+} (0.97 Å) [35]. The calculated lattice parameter values reveal the possibility of presence of Tb in both the oxidation states.

The average crystallite size of $Ce_xTb_{1-x}O_2$ phases present in various samples (Table 1) implies that crystallization of ceria-terbia solid solutions is strongly dependent on the calcination temperature as well as nature of the support. A regular increase in the crystallite size was observed with increasing calcination temperature from 773 to 1073 K. The crystallite size values are however not absolutely considered and TEM-HREM investigations are performed in order to get an unambiguous result.

Please cite this article in press as: A.T. Miah, P. Saikia, Dispersion of nanosized ceria-terbia solid solutions over silica surface: Evaluation of structural characteristics and catalytic activity, Mol. Catal. (2017), http://dx.doi.org/10.1016/j.mcat.2017.11.020

Table 1
BET surface area, crystallite size, and cell 'a' parameter measurements of $CeO_2 - TbO_2/SiO_2$ (CTS) samples calcined at different temperatures.

Sample/Calcination Temperature (K)	BET SA (m^2g^{-1})	Crystallite size (nm)[a]	Cell Parameter 'a' (Å)
CT-773	67	5.5	5.37
CTS-773	170	2.55	5.39
CTS-873	141	3.28	5.38
CTS-973	124	3.83	5.38
CTS-1073	110	5.09	5.39

[a] From the XRD measurements with Scherrer equation.

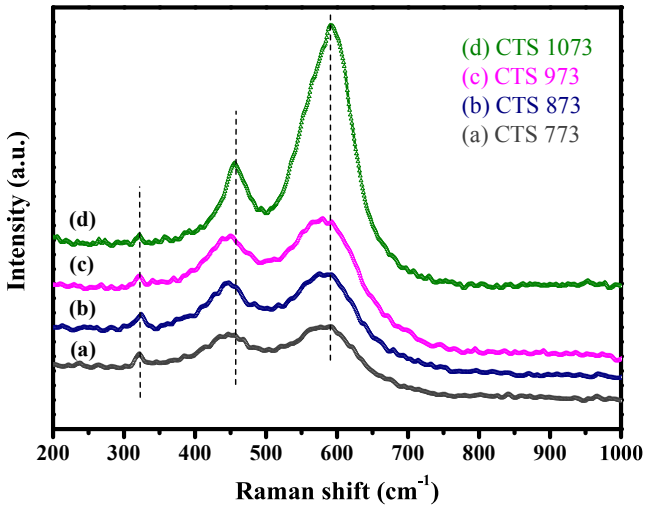

Fig. 2. Raman spectral patterns of $CeO_2 - TbO_2/SiO_2$ (CTS) samples calcined in the temperature region 773–1073 K.

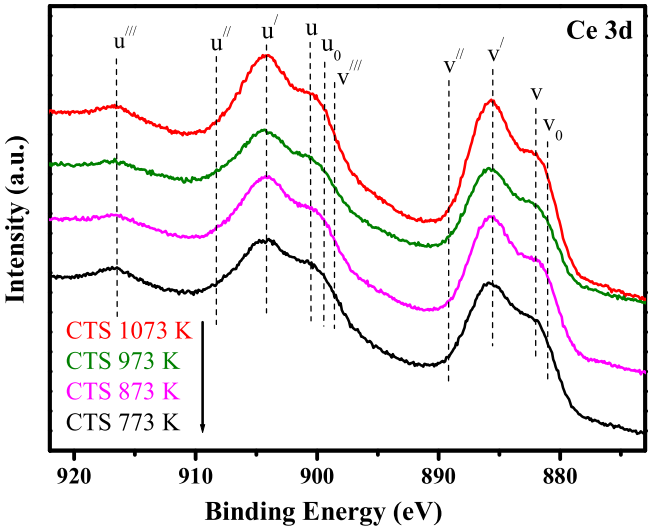

Fig. 3. Ce 3d XP spectra of $CeO_2 - TbO_2/SiO_2$ (CTS) samples calcined at different temperatures.

Fig. 2 presents the Raman spectroscopic results of various samples calcined at different temperatures. Visible Raman analysis of pristine ceria is known to show only one peak at ~462 cm^{-1} due to the F_{2g} Raman-active mode characteristic of the cubic fluorite structure of CeO_2 [3,36]. However, UV-Raman analysis reveals a considerable red shift of this particular peak to ~469 cm^{-1} [3,36]. Presumably, this band shift is caused by a small degree of hydration [37]. As observed, the peak at ~460 cm^{-1} is most prominent for all CTS samples justifying the presence of a cubic $Ce_xTb_{1-x}O_2$ phase. The emergence of additional bands at ~315 and 600 cm^{-1} indicates some distortion of the oxygen sub-lattice. Apparently, the peak at ~600 cm^{-1} is relatively more intense which may be due to the resonance enhancement of the Raman scattering cross section under UV excitation [37]. Interestingly, no Raman lines relating to terbia were observed corroborating with the XRD results. The band at ~460 cm^{-1} is due to symmetric O—Ce—O stretching mode [38].

With increasing calcination temperature the intensity of the F_{2g} band is relatively increased that could be attributed to better crystallization of ceria-terbia solid solution at higher calcination temperatures. The broadness of Raman peaks is due to the presence of silica support as well as small crystallites of Ce-Tb oxide. It is known that the intensity of the Raman band depends on several factors including grain size and morphology [39]. The presence of the pronounced broad band at ~600 cm^{-1} was due to a non-degenerate Raman inactive longitudinal optical mode of ceria which arises due to relaxation of symmetry rules [40,41]. In particular, the substitution of terbium into the ceria lattice with an increase in calcination temperature gives rise to oxygen vacancies, which are responsible for the emergence of this band [42]. The appearance of a weak band at ~315 cm^{-1} was accounted for the displacement of oxygen atoms from their normal lattice positions [38]. Interestingly, these bands gained intensity after calcination at 1073 K, indicating a high disorder of the oxygen sub-lattice in the fluorite structure. Silica did not exhibit any Raman features in line with the results reported in the literature [43]. This observation suggests that silica forms part of the substrate support on which ceria-terbia solid solution is dispersed. The absence of any other Raman features provided one more inference that silica is not forming any compound with cerium and terbium oxides.

UV-vis DRS measurement is carried out for CTS sample calcined at 773 and 1073 K and the patterns are shown in Fig. E2 . Interestingly, this spectroscopic technique could clearly identify nanocrystalline ceria particles of size below 5 nm, which is normally undetectable with XRD investigation [44,45]. As can be seen from Fig. 3, the UV–vis absorption of CeO_2 shows three prominent bands at around 241, 286, and 336 nm. In other words, the absorption solely occurs in the UV region of the electromagnetic spectrum which could be attributed to its large band gap (~3.2 eV) [46]. The absorption band at ~286 nm can be ascribed to $O^{2-} \rightarrow Ce^{4+}$ charge transfer while the band at ~336 nm corresponds to inter-band transitions [47]. The poorly resolved band maxima near ~241 nm is due to $O^{2-} \rightarrow Ce^{3+}$ charge transfer transitions [44]. Another interesting observation can be drawn from the present investigation is that the absorption edges are shifted towards lower wavelengths compared to pristine ceria [7]. However, the occurrence of the charge transfer transitions reveals the existence of cerium in its both oxidation states [48]. More importantly, the $O^{2-} \rightarrow Ce^{3+}$ transitions indicate the formation of oxygen vacancy defects and this observation is intriguingly in agreement with the Raman spectroscopic investigations. Also, no evidence regarding the presence of other phases like TbO_2 could be found in this study in line with both XRD and Raman measurements.

For further confirmation of the DRS observations, XPS measurements were carried out. The O 1s profiles are presented in Fig. E3 . It is evident from the figure that the profiles exhibit an intense and broad photoelectron peak at ~531 eV attributed to the O 1s ionization of the lattice oxygens associated with $Ce_{0.8}Tb_{0.2}O_2$ mixed

Please cite this article in press as: A.T. Miah, P. Saikia, Dispersion of nanosized ceria-terbia solid solutions over silica surface: Evaluation of structural characteristics and catalytic activity, Mol. Catal. (2017), http://dx.doi.org/10.1016/j.mcat.2017.11.020

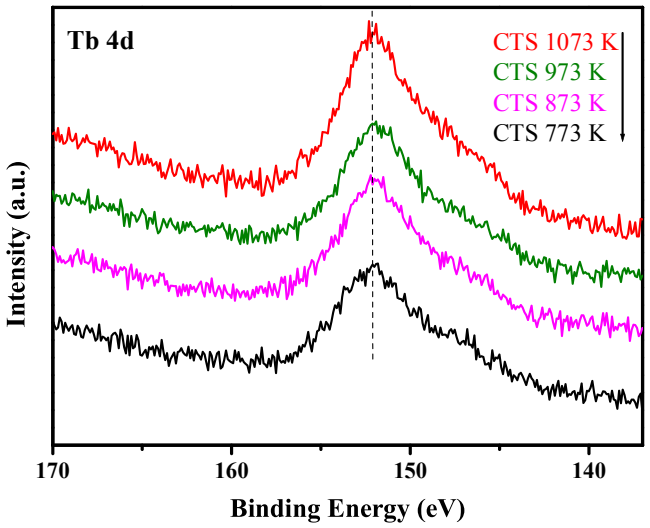

Fig. 4. Tb 4d XP spectra of $CeO_2 - TbO_2/SiO_2$ (CTS) samples calcined at different temperatures.

oxide. With the increase of calcination temperature, though the binding energy values relating to O 1s peak doesn't realize any considerable change, the peak becomes gradually narrow. This is due to better crystallization of the Ce-Tb mixed oxides at higher calcination temperatures. However, the overall results ruled out the possibility of compound formation among the component oxides after 773 K. The Ce 3d photoelectron spectra of the CTS samples were interpreted by means of Burrough's notations [49] and the patterns are presented in Fig. 3. As can be observed from the figure, the Ce 3d spectrum consists of two sets of spin-orbit components namely, $3d_{3/2}$ and $3d_{5/2}$, were represented by the notation u and v respectively. Each of the components shows multiple photoelectron peaks attributed to the final-state effects [9].

Here, the peaks generating from the $3d_{3/2}$ contribution occur at 899 (u_0), 900.5 eV (u), 904.1 eV (u'), 908 eV (u''), and 916.5 eV (u''') whereas that for the $3d_{5/2}$ contribution is observed at 881.1 (v_0), 882 eV (v), 885.4 eV (v'), 889 eV (v''), and 898.5 eV (v'''). The peaks at u and v are the main lines corresponding to the Ce^{4+} state whereas u'', u''', v'', and $v'''$are satellites related to this state. In general, the main signals due to Ce^{3+} state locate at ~881 eV (v_0) and 898 eV (u_0). In the present investigation, the satellites to these features ($v'$and u') could be observed at 885.4 and 904.1 eV, respectively. The absence of a peak at 881 eV reveals that Ce is predominantly in the 4+ oxidation state, which is established by the considerable intensity of the u'''component. However, significant intensity observed around 885 eV confirms the presence of Ce^{3+}. Thus, the prepared samples contain Ce both in the 4+ and the 3+ states. As the calcination temperature increases, the intensity of the peaks at around 885 eV (v') and (u') 904 eV increased and that of the peak at 916 eV (u''') decreased implying a higher amount of Ce^{3+} in the samples calcined at higher temperatures. Fig. 4 shows the Tb 4d core level spectra of the CTS samples. Mention worthy that the assignment of accurate Tb oxidation states in Tb 4d spectra is quite ambiguous due to the very complex nature of the spectral patterns and no appropriate literature could be found. However, it is accorded that in Tb 4d XPS pattern, Tb^{3+} gives a signal below 150 eV, whereas Tb^{4+} is associated with features above 150 eV [3,50]. Here, the spectra are apparently very broad (ranges from 140 to 160 eV) showing the maxima at ~152 eV and a tailing toward 160 eV, suggests the presence of more than one Tb oxidation state. Accordingly, it can be inferred that the CTS composite oxide contains Tb both in the 3+ and 4+ oxidation state. The intensity of the peak maxima is found to be slightly increased with increase in calcination temperature suggesting the presence of Tb^{4+} in relatively higher amounts of than Tb^{3+}.

Fig. E4 shows the core level Si 2p photoelectron spectra of the CTS samples calcined at different temperatures. The binding energy pertaining to the Si 2p spectra exhibits maxima at ~102.2 eV in good agreement with the values reported in the literature [13]. As can be seen from the figure, the spectra are of poor intensity with broaden peak widths giving an impression that silica is almost inaccessible to the surface due to the presence of Ce-Tb oxide over-layers. It is known that the oxidized silicon may be present in different forms such as CeO_{2-x}/SiO_2 [51,52] or as an amorphous silicate layer [53,54], where partial reduction of Ce^{4+} to Ce^{3+} occurs together with partial oxidation of Si. Interestingly, formations of such compound like $CeSiO_4$ or $TbSiO_4$ have not taken place in this study as they reveal the Si 2p binding energy value of 101 eV [55]. This remark is fascinatingly in line with Raman spectroscopic results.

The binding energy (eV) values of O 1s, Ce 3d, Tb 4d, and Si 2p spectra are presented in Table E1. It is clearly revealed that the XPS bands and the corresponding binding energy values are highly sensitive to the calcination temperature and composition of the samples. As presented in Table 2, the atomic ratios for Ce/Tb, Tb/Si, and Ce/Si didn't change considerably with the increase of temperature indicating the conservation of composition. This observation further ubstantiates that no reaction occurred among the components within the temperature range of 773–1073 K.

Electron microscopic investigations are very relevant in investigating the structural features at atomic level. This technique can authenticate the observations of XRD and Raman spectroscopy and endow with precise facts. Considering this, TEM-HRTEM analyses were carried out for the CTS samples. The TEM and HRTEM images pertaining to 773 K and 1073 K calcined samples are shown in Figs. 5 (a), (b) and 6 (a), (b), respectively. The TEM global micrographs revealed agglomerated microstructures of the sample. However, plain faces of crystallites are very rare in the figure, which suggests that maximum share of the material is in amorphous state. Interestingly, the exact morphological views of the particles could be discerned from the HRTEM images. As can be seen from Figs. 5(a) and 6(a), the image indicates the well dispersion of reasonably small particles (with a diameter of ~3–4 nm) over the amorphous silica matrix. However, slight increases in particle size (up to ~5 nm) with temperature increase to 1073 K could be noted (Figs. 5(b) and 6(b)). The shapes of the particles are somewhat cuboctahedral. As observed, the well-defined lattice fringes suggest a high degree of crystallinity that could be obviously attributed to the CeO_2-TbO_2 mixed oxide particles. The mixed oxide particles seem to be attached to each other by certain shared (*i.e.*, overlapped) regions to form larger ensembles. The presence of such regions in the mixed oxide particles might be beneficial for better catalytic performance.

The reduction/oxidation properties pertaining to the 773 K calcined silica supported Ce – Tb-oxide sample was investigated by TPR – TPO method and the results are presented in ESI Fig. E5 (1st TPR-TPO run) and Fig. E6 (2nd TPR-TPO run). The 1 st TPR profile divulges the commencement of reduction at a moderately low temperature of ~473 K having its maximum at 773 K, which can be attributed to the reduction of surface ceria [3,56]. The second peak could be ascribed to the reduction of bulk ceria, starts appearing at ~873 K and shows the maximum at ~973 K [3,56]. In contrast to the very weak TPR signal (at low temperature region) shown by pristine ceria, the CTS sample exhibited a relatively broad TPR peak. This fact may be as a result of the very high surface area of the catalyst sample [57]. Interestingly, characteristic peaks (at ~576, 940, and 993 K) owing to Tb^{4+} to Tb^{3+} transformation couldn't be detected in line with previous reports [3,56]. In the 1st TPO profile (Fig. E5 (b)) of the reduced sample, the reoxidation peak could

Please cite this article in press as: A.T. Miah, P. Saikia, Dispersion of nanosized ceria-terbia solid solutions over silica surface: Evaluation of structural characteristics and catalytic activity, Mol. Catal. (2017), http://dx.doi.org/10.1016/j.mcat.2017.11.020

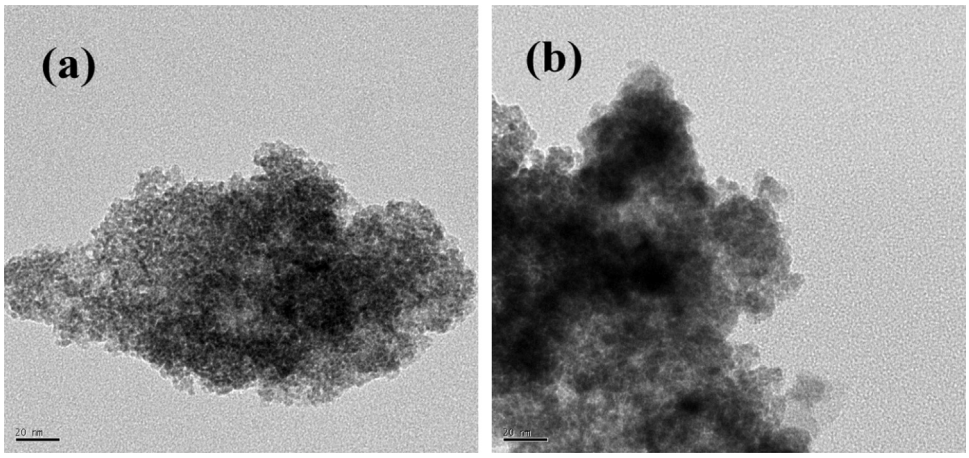

Fig. 5. TEM global pictures of (a) 773 K and (b) 1073 K calcined $CeO_2 - TbO_2/SiO_2$ (CTS) samples.

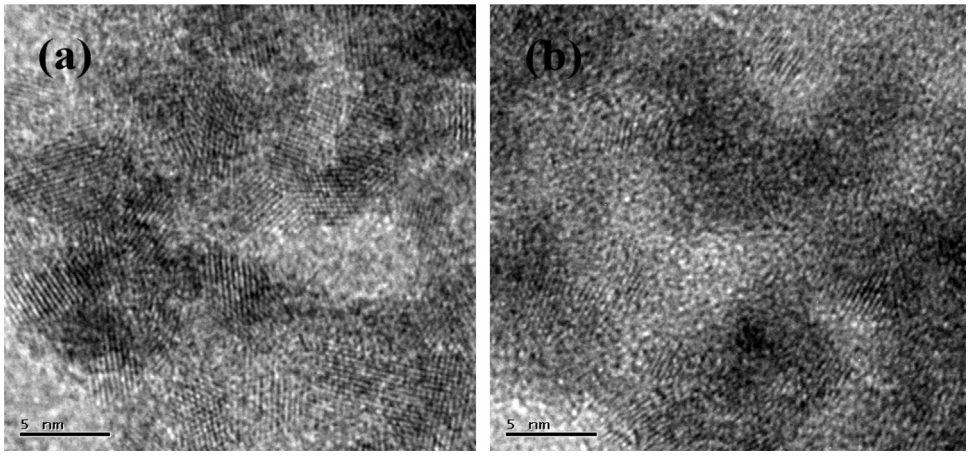

Fig. 6. HRTEM images of (a) 773 K and (b) 1073 K calcined $CeO_2 - TbO_2/SiO_2$ (CTS) samples.

be observed starting at ~373 K and centered at ~473 K. The second prominent reoxidation peak is observed with peak maximum at ~973 K. It is evident from Fig. E6 (a) that the 2nd TPR profile reveals overlapping peaks which could not be resolved. Apparently, the reduction starts at ~673 K and the most prominent reduction peak is centered at ~1073 K indicating a significant increase in the reduction temperature with respect to the 1st TPR run. This is obviously attributable to the increase in particle size and decrease of surface area after treating the sample up to 1073 K. From Fig. E6 (b), it could be seen that the 2nd TPO run results in the occurrence of two distinct reoxidation peaks centered at ~450 and 1000 K that are indicative of the inhomogeneous nature of the catalyst sample. The obtained observations can thus substantiate that the sample is highly thermostable as it maintains good redox activity after severe heat treatment.

The OSC property of the sample calcined at 773 K was measured *via* a thermogravimetric method under cyclic heat treatments in flowing air/nitrogen atmosphere in the temperature range of 573–1073 K was used [58,59]. The thermogram showing the weight loss in the second heat cycle is presented in ESI (Fig. E7). The OSC of the sample was found to be 348.06 μmoles O_2/g ceria (272.5 μmoles O_2/g Ce-Tb-oxide) which is higher than that of the unsupported Ce-Tb mixed oxide. This obtained value is due to the 0.65% weight loss in the second heat cycle of the measurement. In terms of oxygen vacancy concentration (δ), the corresponding value would be 0.21. Several factors may affect the OSC value, such as surface area, particle size, method of preparation, and nature of supporting oxide etc. The exact role of these parameters is still not completely understood. However, it is clear from the analysis of these parameters that the OSC is not substantially improved by small particle size or high specific surface area. Though CTS bears a very high specific surface area and very small crystallite size the OSC value is not so high for this sample. This leads us to conclude that to get high OSC, the bulk oxygen diffusion rate must be sufficiently large and the observed OSC is controlled by thermodynamic equilibrium of the redox reaction [60].

3.2. Catalytic activity studies

Catalytic activity correlating the acid-base and redox behavior of the synthesized samples was evaluated for dehydration of 4-methylpentan-2-ol at normal atmospheric pressure and temperatures ranging from 523 to 673 K in N_2 stream. As the chosen reaction temperatures are reasonably lower than that used for the calcination of the samples, so the detailed study was carried out with the sample calcined at 773 K. However, to know the influence of structural characteristics on the catalytic performance, all CTS samples were employed only for investigating the amount of conversion. With increasing calcination temperature from 773 to 1073 K, the conversion efficiency was observed to be slightly decreased in every interval of 100 K. This may be an effect of the bigger particles of Ce–Tb-oxide crystallites formed due to the heat treatment at higher calcination temperatures. The dehydration/conversion patterns as a function of time-on-stream

Please cite this article in press as: A.T. Miah, P. Saikia, Dispersion of nanosized ceria-terbia solid solutions over silica surface: Evaluation of structural characteristics and catalytic activity, Mol. Catal. (2017), http://dx.doi.org/10.1016/j.mcat.2017.11.020

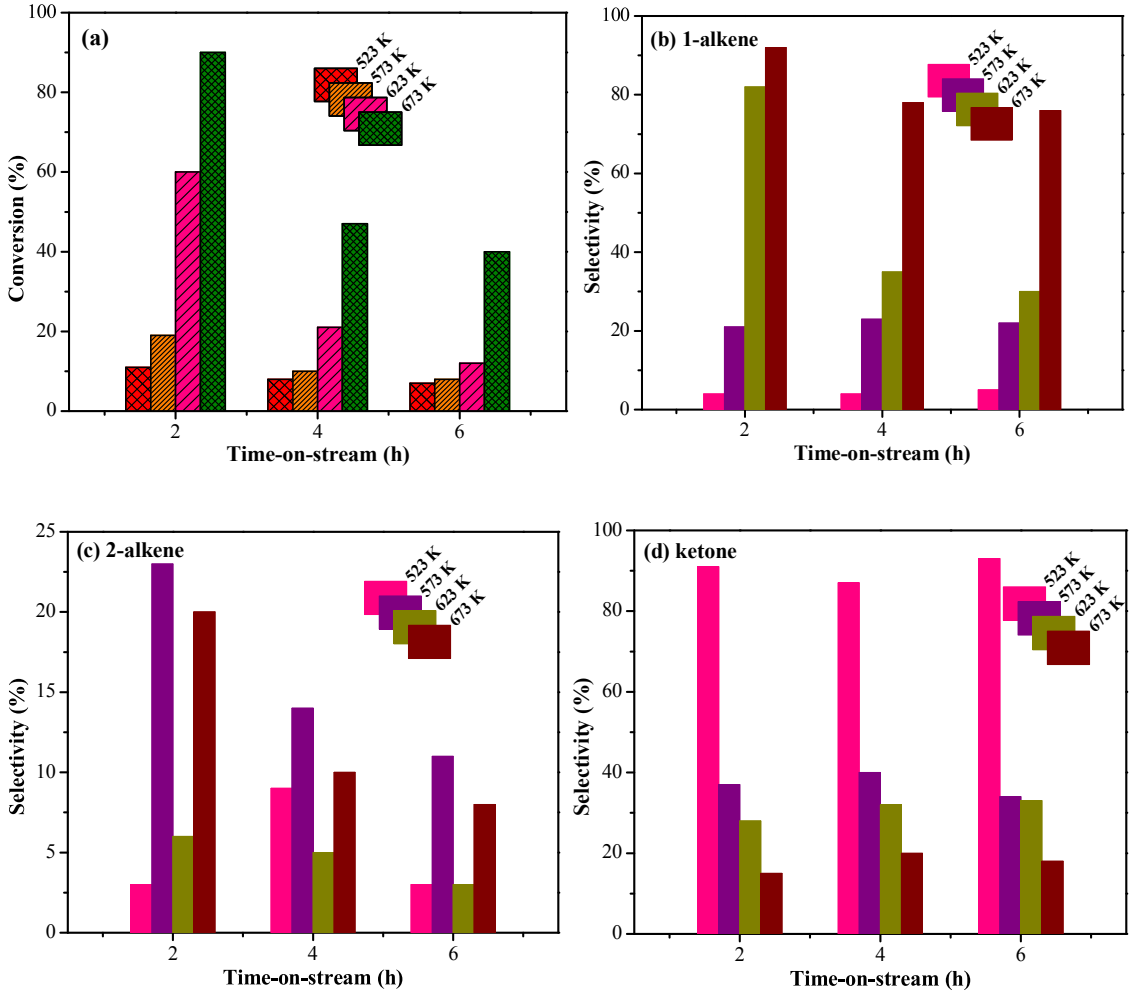

Fig. 7. Conversion of 4-mentylpentan-2-ol (a) and product selectivity to (b) 1-alkene (4-methylpent-1-ene), (c) 2-alkene (4-methylpent-2-ene), and (d) ketone (4-methylpentan-2-one) *vs.* time-on-stream over ceria–terbia (CT 773) solid solution at different reaction temperatures.

at different reaction temperatures over CT and CTS (calcined at 773 K) samples are summarized in Figs. 7 and 8, respectively. It is observed from the figures that CTS sample outperform the catalytic alcohol conversion activity as well as selectivity (towards the formation of desired product, 1-alkene) of CT sample regardless of the reaction parameters (*i.e.*, time-on-stream and reaction temperatures). When CTS demonstrated complete conversion of the alcohol reactant (reaction conditions: temperature 623 K, time 2 h), CT showed a conversion of only 60%. These observations clearly reveal the effect of dispersion of CT over the surface of SiO_2 support. Though relatively better alcohol conversion activity is noted at initial reaction time (2 h), the initial reaction temperatures on the contrary revealed low conversion for both the catalysts. The low conversion may be attributed to the substandard activation of the alcohol at such temperature regime. Intriguingly, the conversion is substantially improved with gradual increase in reaction temperature and decreased with reaction time. [22,24,25]. Mention worthy that our CTS catalyst revealed higher alcohol conversion activity in comparison to the previously reported similar catalyst systems [4,22,25].

The catalytic dehydration of 4-methylpentan-2-ol is known to endow with different products with varying compositions. The composition of the product mixture relies on the mechanistic route of the reaction occurs on the surface of the catalyst. Generally, three different mechanistic routes (*i.e.*, E1cB, E2 and E1) could be envisaged for dehydration of alcohols [4,24,25]. But the specific route which is to be prevailed depends largely on the compositions, surface characteristics, and acid-base and redox behavior of the catalytic materials employed [4,25]. However, due to the possibility of arising intermediate situations, these mechanisms may not be surely involved and hence, should be considered as limiting cases.

It is believed that E1cB mechanism operates *via* the formation of carbanion when weak acidic sites are weak and basic sites are strong enough. This mechanistic route gives major product 1-alkene (Hofmann product) accompanied by the formation of small amount of ketones due to unavoidable side reactions. The E1 route on the contrary proceeds *via* the carbocation intermediate formation and gives undesired 2-alkene as the major product. This route is prevailed when excess amount of acidic sites are present on the catalyst surface. However, formation of ketones can also be witnessed if the catalyst surface is enriched with basic sites. The E2 route doesn't entail the formation of any intermediate (*i.e.*, carbanion or carbocation) and hence, follows a concerted mechanism. This route is operated at comparable strengths of the acid and base sites that in fact inhibit intermediate formation. In this case, the reactant species are converted into a mixture product containing notably higher amount of 2-alkene (Saytzeff product) than the preferred product, 1-alkene [24,61].

It is evident that the selectivity to 1-alkene (4-methylpent-1-ene) is more prominent with CTS than that with CT irrespective of both the reaction parameters. Also, the 1-alkene selectivity is reg-

Please cite this article in press as: A.T. Miah, P. Saikia, Dispersion of nanosized ceria-terbia solid solutions over silica surface: Evaluation of structural characteristics and catalytic activity, Mol. Catal. (2017), http://dx.doi.org/10.1016/j.mcat.2017.11.020

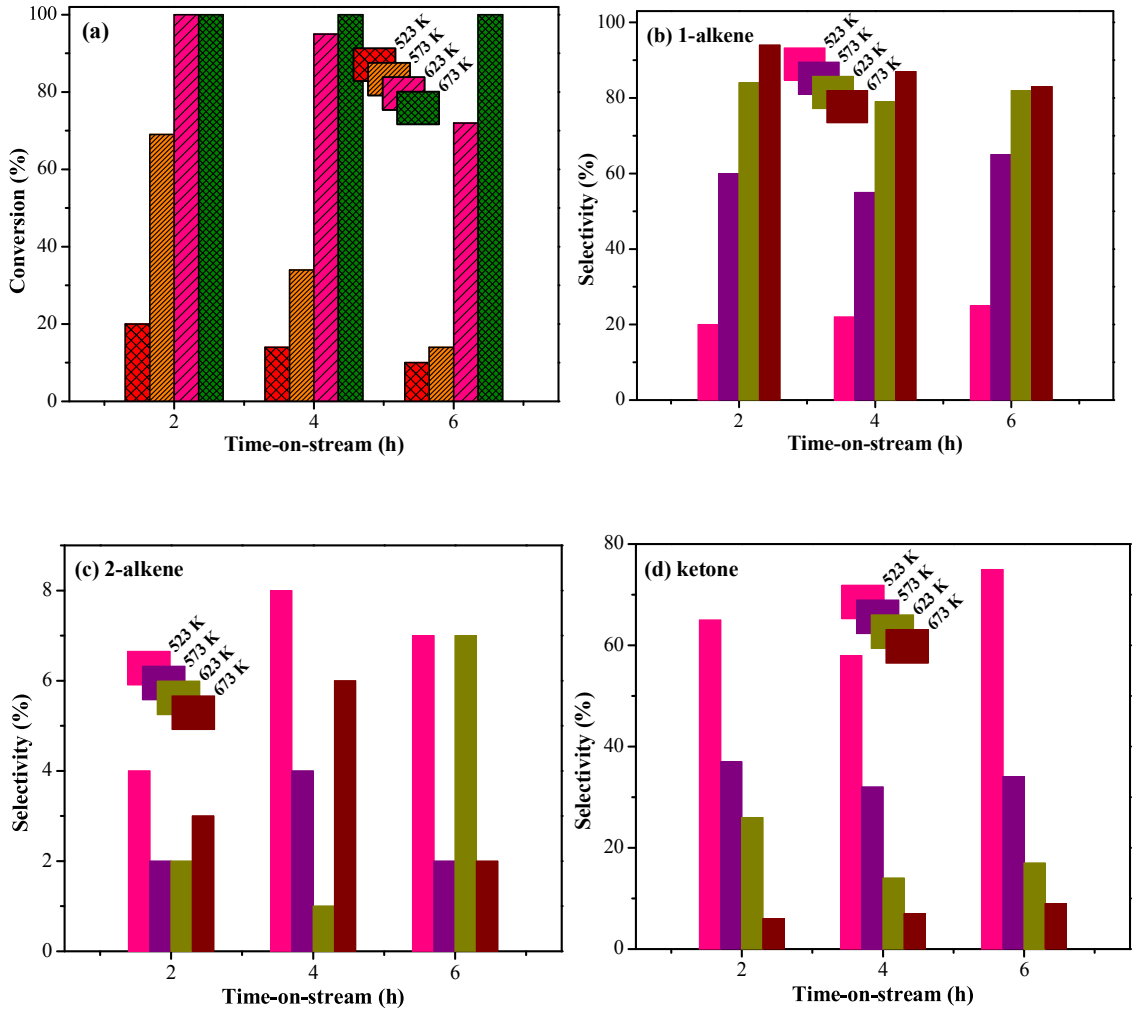

Fig. 8. Conversion of 4-mentylpentan-2-ol (a) and product selectivity to (b) 1-alkene (4-methylpent-1-ene), (c) 2-alkene (4-methylpent-2-ene), and (d) ketone (4-methylpentan-2-one) *vs.* time-on-stream over silica supported ceria–terbia (CTS 773) solid solution at different reaction temperatures.

ularly increased with the increase of reaction temperature for both the catalysts. However, this trend is not absolutely followed with increasing reaction time. Interestingly, the selectivity to 2-alkene (4-methylpent-2-ene) is nominal for both the catalysts at all reaction conditions and is reasonably decreased when CTS is employed in lieu of CT. At the low reaction temperature (*i.e.*, 523–573 K) regime, though the selectivity to ketone, *i.e.*, 4-methylpentan-2-one (for all reaction time) is considerable, it was found to be decreased recurrently upon increase in reaction temperature. This temperature dependent decrease is extremely higher with CTS in comparison to CT. The selectivity to ketone (4-methylpentan-2-one) is observed to be lowered drastically for CTS with respect to CT in terms of both the reaction parameters and become almost negligible at the highest temperature (*i.e.*, 673 K) investigated. The negligible amount of 2-alkene and ketone formation suggests that the dehydration of 4-methylpentan-2-ol proceeds through an E1cB mechanism. Thus, it could be surmised that the dehydration of 4-methylpent-2-ol is most favorable at 673 K from the standpoint of both conversion and selectivity. The above observations could be correlated to the structural features of highly dispersed Ce–Tb-oxides over SiO_2 with balanced acid-base and redox sites [4,25]. In short, the better conversion efficiency as well as selectivity of the CTS catalyst may be due to the formation of smaller Ce–Tb crystallites of size ~3–4 nm, augmented surface oxygen vacancies (*i.e.*, improved redox behavior) and hence more Ce^{3+} ion concentration. In other words, we can say that dispersion of ceria-terbia over amorphous silica results in improved acid-base and redox properties which lead to an enhancement in the conversion of the reactant alcohol and also the selectivity towards the desired product, 1-alkene. In addition to catalytic efficiency and selectivity, stability is often regarded as an enviable aspect of any catalyst system. Interestingly, the CeO_2-TbO_2/SiO_2 composite catalyst revealed outstanding stability against deactivation which was confirmed from the uniform performance of the catalyst during time-on-stream experiments. Literatures on ceria-based mixed oxides, especially ceria-terbia combinations are known to be highly coke resistant and exhibit promising stability against deactivation during time-on-stream runs for various reactions [3,25,56,62]. This was primarily attributed to the availability of lattice oxygen owing to oxygen storage and release property of the Ce–Tb-oxides [3,56,62]. Therefore, the present study indicates that amorphous silica can be used as an inert support to stabilize Ce–Tb-oxide nanocrystallites against sintering at elevated temperatures for achieving better catalytic activity as well as selectivity. However, the nature of acid-base sites of the prepared catalysts and their exact role on the conversion and selectivity are still not fully clear and hence, undeniably it demands exhaustive investigations which are in active progress.

Please cite this article in press as: A.T. Miah, P. Saikia, Dispersion of nanosized ceria-terbia solid solutions over silica surface: Evaluation of structural characteristics and catalytic activity, Mol. Catal. (2017), http://dx.doi.org/10.1016/j.mcat.2017.11.020

4. Conclusions

In summary, this work reports the fabrication of a novel catalyst system based on the dispersion of nanosized CeO_2-TbO_2 over SiO_2 surface *via* a soft chemical route namely, deposition co-precipitation. Calcination temperature is revealed to play vital role on the structural features of the CeO_2-TbO_2/SiO_2 samples. The catalyst samples exhibited high thermal stability, specific surface area and better redox as well as acid-base characteristics. XRD, Raman spectroscopy, UV–vis DRS, and XPS studies corroborate the absence of formation of any compound between silica and the oxides of cerium and terbium. Besides, the Raman spectroscopy measurements indicate pronounced substitution of terbium into the ceria lattice with increasing calcination temperature, thereby generating more oxygen vacancies, lattice defects and displacement of oxygen ions from their normal lattice positions. XRD and TEM studies reveal a regular increase in the Ce–Tb crystallite size with increase in calcination temperature from 773 to 1073 K. UV–vis DRS and XPS measurements substantiate the existence of Ce and Tb in their both oxidation states namely 3+ and 4+. The patterns of the spectra suggest the presence of trivalent component in relatively higher amounts than their tetravalent counterparts for both the elements. The OSC of CeO_2-TbO_2/SiO_2 sample was found to be significantly high owing to the formation of solid solution and higher defect sites in its crystal lattice, higher dispersion of the active phase over the support, and easy reducibility. The CeO_2-TbO_2/SiO_2 samples showed remarkably improved catalytic activity for dehydration of 4-methylpentan-2-ol in terms of total conversion and selectivity towards 4-methylpent-1-ene compared to the CeO_2-TbO_2 sample. The improved activity of CeO_2-TbO_2/SiO_2 composite oxides is due to the formation of more oxygen vacancy sites in its crystal structure, surface enrichment of Ce^{3+} ions, better redox properties and well balanced acid-base sites. Above all, the better redox property and well balanced acid-base sites of CeO_2-TbO_2/SiO_2 composite oxides might be beneficial for many catalytic reactions. Also, the high thermo-stability of the composite oxide opens up the avenues for high temperature applications.

Acknowledgements

Authors like to thank DST, Govt. of India for Project Grant No. SR/FT/CS-69/2011. Help from Prof. W. Gruenert, Ruhr Universitat, Bochum, Germany is gratefully acknowledged.

Appendix A. Supplementary data

Supplementary data associated with this article can be found, in the online version, at http://dx.doi.org/10.1016/j.mcat.2017.11.020.

References

[1] T. Montini, M. Melchionna, M. Monai, P. Fornasiero, Chem. Rev. 116 (2016) 5987.
[2] C. Sun, H. Li, L. Chen, Energy Environ. Sci. 5 (2012) 8475–8505.
[3] B.M. Reddy, P. Saikia, P. Bharali, S.-E. Park, M. Muhler, W. Grunert, J. Phys. Chem. C 113 (2009) 2452.
[4] P. Bharali, G. Thrimurthulu, L. Katta, B.M. Reddy, J. Ind. Eng. Chem. 18 (2012) 1128.
[5] D. Devaiah, D. Jampaiah, P. Saikia, B.M. Reddy, J. Ind. Eng. Chem. 20 (2014) 444.
[6] B.M. Reddy, P. Saikia, P. Bharali, L. Katta, G. Thrimurthulu, Catal. Today 141 (2009) 109.
[7] B.M. Reddy, P. Bharali, G. Thrimurthulu, P. Saikia, L. Katta, S.-E. Park, Catal. Lett. 123 (2008) 327.
[8] M.G. Cutrufello, I. Ferino, E. Rombi, V. Solinas, G. Colon, J.A. Navio, React. Kinet. Catal. Lett. 79 (2003) 93.
[9] A.T. Miah, B. Malakar, P. Saikia, Catal. Lett. 146 (2016) 291.
[10] Z. Zhang, Y. Wang, J. Lu, C. Zhang, M. Wang, M. Li, X. Liu, F. Wang, ACS Catal. 6 (2016) 8248.
[11] N. Pal, E.-B. Cho, A.K. Patra, D. Kim, ChemCatChem 8 (2016) 285.
[12] A.T. Miah, S.K. Bharadwaj, P. Saikia, Powder Technol. 315 (2017) 147.
[13] B.M. Reddy, P. Saikia, P. Bharali, Catal. Surv. Asia 12 (2008) 214.
[14] Z. Wu, A.K.P. Mann, M. Li, S.H. Overbury, J. Phys. Chem. C 119 (2015) 7340.
[15] Z. Hu, H. Metiu, J. Phys. Chem. C 116 (2012) 6664.
[16] E.W. McFarland, H. Metiu, Chem. Rev. 113 (2013) 4391.
[17] L. Vivier, D. Duprez, ChemSusChem 3 (2010) 654.
[18] N. Pal, E.-B. Cho, D. Kim, C. Gunathilake, M. Jaroniec, J. Chem. Eng. 262 (2015) 1116.
[19] N. Pal, E.-B. Cho, D. Kim, M. Jaroniec, J. Phys. Chem. C 118 (2014) 15892.
[20] M. Tamura, S.M.A.H. Siddiki, K.-I. Shimizu, Green Chem. 15 (2013) 1641.
[21] M.G. Cutrufello, I. Ferino, R. Monaci, E. Rombi, V. Solinas, Top. Catal. 19 (2002) 225.
[22] B.M. Reddy, G. Thrimurthulu, P. Saikia, P. Bharali, J. Mol. Catal. A: Chem. 275 (2007) 167.
[23] V. Solinas, E. Rombi, I. Ferino, M.G. Cutrufello, G. Colon, J.A. Navio, J. Mol. Catal. A: Chem. 204–205 (2003) 629.
[24] L. Katta, P. Sudarsanam, B. Mallesham, B.M. Reddy, Catal. Sci. Technol. 2 (2012) 995.
[25] B.M. Reddy, P. Lakshmanan, P. Bharali, P. Saikia, J. Mol. Catal. A: Chem. 258 (2006) 355.
[26] B.M. Reddy, P. Lakshmanan, A. Khan, S. Loridant, C.L. Cartes, T.C. Rojas, A. Fernández, J. Phys. Chem. B 109 (2005) 13545.
[27] K. Kenevey, F. Valdivieso, M. Soustelle, M. Pijolat, Appl. Catal. B: Environ. 2 (2001) 93.
[28] E. Rocchini, A. Trovarelli, J. Liorca, G.W. Graham, W.H. Weber, M. Maciejewski, A. Baiker, J. Catal. 194 (2000) 461.
[29] B. Kucharczyk, W. Tylus, L. Kepinski, Appl. Catal. B: Environ. 49 (2004) 27.
[30] C. Bozo, F. Gaillard, N. Guilhaume, Appl. Catal. A: Gen. 220 (2001) 69.
[31] G. Colon, M. Pijolat, F. Valdivieso, H. Vidal, J. Kaspar, E. Finocchio, M. Daturi, C. Binet, J.C. Lavalley, R.T. Baker, S. Bernal, J. Chem. Soc. Faraday Trans. 94 (1998) 3717.
[32] R.D. Shannon, Acta Crystallogr. A 32 (1976) 751.
[33] S. Meriani, G. Spinolo, Powder Diffract. 2 (1987) 255.
[34] B.D. Cullity, Elements of X-ray Diffraction, Addison-Wesley, Reading, MA, 1956.
[35] A.B. Hungria, A.M. Arias, M.F. Garcia, A.I. Juez, A.G. Ruiz, J.J. Calvino, J.C. Conesa, J. Soria, Chem. Mater. 15 (2003) 4309.
[36] B.M. Reddy, A. Khan, Catal. Surv. Asia 9 (2005) 155.
[37] Y.T. Chua, P.C. Stair, I.E. Wachs, J. Phys. Chem. B 105 (2001) 8600.
[38] M. Yashima, H. Arashi, M. Kakihana, M. Yoshimura, J. Am. Ceram. Soc. 77 (1994) 1067.
[39] J.E. Spanier, R.D. Robinson, F. Zhang, S.W. Chan, I.P. Herman, Phys. Rev. B 64 (2001) 245407.
[40] L.-M. Lin, L.-P. Li, G.-S. Li, W.-H. Su, Mater. Chem. Phys. 69 (2001) 236.
[41] W.H. Weber, K.C. Hass, J.R. McBride, Phys. Rev. B 48 (1993) 178.
[42] J.R. McBride, K.C. Hass, B.D. Poindexter, W.H. Weber, J. Appl. Phys. 76 (1994) 2435.
[43] I.E. Wachs, F.D. Hardcastle, S.S. Chan, Spectroscopy 1 (1986) 30.
[44] A. Bensalem, F.B. Verduraz, M. Delamar, G. Bugli, Appl. Catal. A: Gen. 121 (1995) 81.
[45] M.I. Zaki, G.A.M. Hussein, S.A.A. Mansour, H.M. Ismail, G.A.H. Mekhemer, Colloids Surf. A 127 (1997) 47.
[46] S.A. Ansari, M.M. Khan, M.O. Ansari, S. Kalathil, J. Lee, M.H. Cho, RSC Adv. 4 (2014) 16782.
[47] A. Bensalem, J.C. Muller, F.B. Verduraz, J. Chem. Soc. Faraday Trans. 88 (1992) 153.
[48] P. Saikia, A.T. Miah, P.P. Das, J. Chem. Sci. 129 (2017) 81.
[49] A. Burroughs, A. Hamnett, A.F. Orchard, G. Thornton, J. Chem. Soc. Dalton Trans. 1 (1976) 1686.
[50] G. Blanco, J.M. Pintado, S. Bernal, M.A. Cauqui, M.P. Corchado, A. Galtayries, J. Ghijsen, R. Sporken, T. Eickhoff, W. Drube, Surf. Interface Anal. 34 (2002) 120.
[51] A. Galtayries, M. Crucifix, G. Blanchard, G. Terwagne, R. Sporken, Appl. Surf. Sci. 142 (1999) 159.
[52] H. Nagata, M. Yoshimoto, T. Tsukahara, S. Gonda, H. Koinuma, Mater. Res. Soc. Symp. Proc. 202 (1991) 445.
[53] T. Inoue, Y. Yamamoto, M. Satoh, A. Ide, S. Katsumata, Thin Solid Films 281 (1996) 24.
[54] F. Sanchez, M. Varela, C. Ferrater, M.V.G. Cuenca, R. Aguiar, J.L. Morenza, Appl. Surf. Sci. 70 (1993) 94.
[55] H. Behner, J. Wecker, T. Mathee, K. Samwer, Surf. Interf. Anal. 18 (1992) 685.
[56] B.M. Reddy, P. Saikia, P. Bharali, Y. Yamada, T. Kobayashi, M. Muhler, W. Grunert, J. Phys. Chem. C 112 (2008) 16393.
[57] P.W. Dunne, A.M. Carnerup, A. Węgrzyn, S. Witkowski, R.I. Walton, J. Phys. Chem. C 116 (2012) 13435.
[58] M. Ozawa, K. Matuda, S. Suzuki, J. Alloys Compd. 56 (2000) 303.
[59] M. Ozawa, C.K. Loong, Catal. Today 50 (1999) 329.
[60] E. Aneggi, M. Boaro, C. de Leitenburg, G. Dolcetti, A. Trovarelli, J. Alloys Compd. 408-412 (2006) 1096.
[61] M.G. Cutrufello, I. Ferino, R. Monaci, E. Rombi, G. Colon, J.A. Navio, Phys. Chem. Chem. Phys. 3 (2001) 2928.
[62] B.M. Reddy, P. Lakshmanan, S. Loridant, Y. Yamada, T. Kobayashi, C.L. Cartes, T.C. Rojas, A. Fernandez, J. Phys. Chem. B 110 (2006) 9140.

Please cite this article in press as: A.T. Miah, P. Saikia, Dispersion of nanosized ceria-terbia solid solutions over silica surface: Evaluation of structural characteristics and catalytic activity, Mol. Catal. (2017), http://dx.doi.org/10.1016/j.mcat.2017.11.020